University of Anbar

Anbar Journal of Engineering Science

journal homepage: https://ajes.uoanbar.edu.iq/

Influence of Inner Cylinder Rotation and Eccentricity on Convective Heat Transfer in Power-Law Non-Newtonian Flow within Annular Cylinders

Mohammed Y. Mahmood[a], Waleed M. Abed[b]
[a,b] *Mechanical Engineering Department/ University of Anbar, Anbar, Iraq*
Email: Moh23e2001@uoanbar.edu.iq   ; *ORCID: https://orcid.org/0009-0002-9813-1369*
Email: waleed_eng76@uoanbar.edu.iq   ; *ORCID: https://orcid.org/0000-0001-7971-189X*

PAPER INFO	ABSTRACT
  	The annular geometry with inner cylinder eccentricity and rotation is significant in many thermal and engineering fields, particularly with non-Newtonian fluid flows. A numerical analysis examines the effects of rotation and eccentricity of the inner cylinder on the fluid flow and heat transfer characteristics of shear-thinning non-Newtonian fluids within annular geometry under developing steady laminar flow. The computational model simulates non-Newtonian annular flow using a power-law viscosity model for generalized Reynolds numbers ($100 \leq Re_g \leq 1000$), flow behavior index ($0.2 \leq n \leq 0.8$), and Taylor number Ta = 10^4 with radius ratio $r^* = 0.5$. The simulation employs hydraulic and thermal boundary conditions, including an adiabatic outer cylinder and a constant temperature at the inner rotating cylinder, while the outer cylinder remains stationary. Results show that axial flow at $n = 0.2$ exhibits lower flow resistance and enhances convective transport compared to higher $n = 0.8$, especially for the concentric case ($\varepsilon = 0$). However, increasing eccentricity from *The $\varepsilon = 0.2$ to $\varepsilon = 0.6$ range alters the heat transfer behavior, with $n = 0.8$ yielding the highest Nusselt numbers at $\varepsilon = 0.6$, due to the* strong secondary flows and intensified local acceleration in the narrow gap. These outcomes reveal that heat transfer enhancement is not solely governed by flow resistance but is also influenced by secondary flows, boundary layer stability, and localized acceleration effects.

1   Introduction

Fluids are broadly categorized into two key types: Newtonian and non-Newtonian. While Newtonian fluids maintain a constant viscosity independent of the shear rate, non-Newtonian fluids exhibit viscosity that varies with the applied shear rate, which leads to more complex and non-linear flow behavior. [1-3]. The GNF (Generalized Newtonian

Fluid) formulation describes a subclass of non-Newtonian fluids where viscosity is time-independent. [4, 5]. Standard mathematical models used for these fluids include the Power-Law, Carreau, Ellis, Bingham, and Cross models. [6-9]. Investigating the flow dynamics of non-Newtonian fluids and their convective heat transfer characteristics in annular geometries is crucial for various engineering applications, including

---

* Corresponding author: Mohammed Y. Mahmood; Email*: Moh23e2001@uoanbar.edu.iq*

polymer processing, lubrication systems, drilling operations, heat exchangers, biomedical devices, and the pharmaceutical industry. [10-12]. Annular configurations, particularly those involving inner cylinder rotation, introduce centrifugal forces, Taylor vortices, and secondary flow patterns, which significantly impact heat transfer. [13-17]. The power-law model, introduced by Ostwald and de Waele [4], is commonly employed to characterize the viscosity of purely viscous non-Newtonian fluids, particularly those that exhibit shear-thinning ($n < 1$) or shear-thickening ($n > 1$) properties. It accurately captures the shear-thinning region but neglects Newtonian plateaus at extreme shear rates. The model is expressed as:

$$\mu = K(\dot{\gamma})^{n-1} \tag{1}$$

where μ is dynamic viscosity, K denotes the fluid consistency coefficient, $\dot{\gamma}$ refers to the shear rate, and n indicates the flow behavior index. Escudier et al. [18] experimentally investigated shear-thinning non-Newtonian fluid flow in a fully developed concentric annulus (radius ratio 0.5) across laminar, transitional, and turbulent regimes. They measured axial velocity, turbulence intensity, and friction factors for (CMC) sodium carboxymethylcellulose, Xanthan gum, and a Laponite/ CMC blend, comparing them to a Newtonian glucose syrup-water mixture. While the Newtonian fluid followed conventional friction factor trends, CMC exhibited shear-thinning with drag reduction. Xanthan gum demonstrated anomalous *fRe* behavior due to elasticity, whereas the Laponite/CMC blend exhibited thixotropic deviations from expected trends. Escudier and Gouldson [19] examined Newtonian and shear-thinning fluid flow within a concentric annular duct having a radius ratio of (0.506) with a rotating centerbody. Using LDA and pressure measurements, they analyzed velocity, turbulence, and friction factors. Rotation increased friction in laminar flow, while axial velocity fluctuations decreased in turbulence. The polymeric fluid showed drag reduction, with Taylor vortices forming at low Reynolds numbers. Escudier et al. [10] conducted a numerical study on fully developed laminar non-Newtonian flow in annuli, incorporating the effects of eccentricity and inner-cylinder rotation using the finite volume technique. They examined friction factors, pressure drop, and velocity distribution for power-law, Herschel-Bulkley, Cross, and Carreau models across a range of Reynolds numbers (10–1000), eccentricity ratios (0–0.98), and radius ratios (0.2–0.8). Results showed increased pressure drop with higher

eccentricity, reduced friction factors for shear-thinning fluids, and velocity concentration in narrow regions near the inner cylinder. The behavior of the fully developed laminar flow of shear-thinning fluids was examined in concentric and highly eccentric (80%) annuli both in the presence and absence of inner cylinder rotation by Escudier et al. [20] used numerical (FVM) and experimental (LDA) methods. For Re_g = 228–332 and Ta = 2026–6020, they analyzed solutions of 0.1% CMC and 0.1% Xanthan gum. Without rotation, axial velocity was uniform with stable shear stress. Rotation shifted tangential velocity inward, slightly increasing shear stress. Eccentricity caused asymmetric velocity profiles and recirculation zones during rotation. Sefid and Izadpanah [21] performed a numerical analysis of both developing and fully developed laminar flow of power-law non-Newtonian fluids with forced convection in concentric annular cylinders. They analyzed the power-law index (0.2–1.8), Reynolds numbers (10–1000), and aspect ratios (0.2, 0.5, 0.8), focusing on velocity, friction factor, developing length, and Nusselt number under different thermal conditions. he results demonstrated that shear-thinning fluids improved convective heat transfer performance and reduced pressure drop. Lower power-law indices resulted in decreased friction factors and increased Nusselt numbers, thereby improving thermal performance with minimal pressure loss. Manglik and Fang [22] numerically studied the forced convection of laminar flow power-law fluids within eccentric annular geometries. For aspect ratios ($0.2 \le r^* < 0.8$), eccentricities ($0 \le \varepsilon \le 0.6$), and flow indices ($0.2 \le n \le 1.8$), they analyzed velocity, temperature, Nusselt numbers, and friction factors. Shear-thinning fluids had flatter velocity profiles, while shear-thickening fluids showed sharper ones. Eccentricity increased velocity gradients, reduced friction, and enhanced Nusselt numbers at higher values. Manglik and Prusa [23] studied viscous dissipation effects on convective heat transfer in thermally developing flows of power-law fluids in tubes with constant wall temperature using finite difference methods. Their results, accurate within 0.3%, showed that decreasing the flow behavior index (n) increases the wall temperature gradient. Under heating, viscous dissipation causes an initial rise in the gradient, unlike non-dissipative fluids. The Nusselt number, influenced by bulk temperature development, becomes unbounded when it matches the wall temperature, limiting its effectiveness as a heat transfer measure. Salubi et

al. [24] conducted an analytical and numerical study on the laminar flow of Newtonian and non-Newtonian fluids (power-law and Herschel–Bulkley models) within concentric and eccentric annuli, with and without inner pipe rotation. By varying eccentricity (0–0.9), rotational speed (0–320 rpm), and flowrate (10–70 m^3/h), they demonstrated that both eccentricity and pipe rotation can significantly reduce pressure drop, particularly for shear-thinning fluids under low flow conditions. Ershadnia et al. [25] developed a combined numerical and data-driven (ANN-based) framework to model non-Newtonian Carreau fluid flow in rotating annular domains. Their analysis demonstrated that increasing rotation rate and radius ratio enhances the shear rate and secondary flow intensity. The ANN model accurately predicted flow behavior and pressure gradients, showing high agreement with the physics-based Navier–Stokes solver. Fusi et al. [26] theoretically examined the secondary flow of an elasto-visco-plastic fluid in a slightly eccentric annulus. Using asymptotic analysis, they demonstrated that eccentricity generates first-order vortices, with flow behavior influenced by the Reynolds and Bingham numbers, viscoelasticity, and the rotational direction. Many experimental and numerical efforts have recently been reported that use the elastic turbulence of non-Newtonian flow with various polymeric viscoelastic fluids and flow geometries to enhance convective heat transfer performance; examples include an axisymmetric swirling (von Karman) flow [27-29] and flow within a square serpentine channel [30-32].

Despite the significant industrial relevance of shear-thinning non-Newtonian fluids in annular geometries with inner cylinder rotation, most existing studies have concentrated primarily on flow behavior under fully-developed conditions, often neglecting the thermal development and heat transfer characteristics. To address this gap, the present study numerically investigates the combined effects of inner cylinder rotation, eccentricity, and rheological properties on both velocity fields and convective heat transfer under developing laminar flow conditions. The simulations are performed using the power-law model and conducted under realistic thermal boundary conditions, the constant temperature at the inner wall and adiabatic outer wall, covering a wide range of parameters: flow behavior index ($0.2 \leq n \leq 0.8$), generalized Reynolds number ($100 \leq Re_g \leq 1000$), eccentricity ($\varepsilon = 0.2, 0.4, 0.6$), and Taylor number ($Ta \leq 104$). The study aims to provide comprehensive insights into the interplay between non-Newtonian rheology, rotational effects, and geometric asymmetry in annular configurations. This integrated approach, which captures both flow and thermal development under combined rotational and eccentric conditions, distinguishes the present work from existing studies and constitutes its main novelty. In summary, the identified research gaps motivated the present numerical investigation, as detailed in the next section.

2   Numerical solution

Numerical simulations in ANSYS Fluent 2021R1 using the Finite Volume Method (FVM) to solve the governing equations of continuity, momentum, and energy for fluid flow and convective heat transfer within eccentric annular cylinders; the Power-law model was adopted in this study due to its well-established capability to describe shear-thinning non-Newtonian fluids. This approach has been widely employed in previous numerical studies dealing with annular geometries. Moreover, the chosen configuration and boundary conditions reflect real-world engineering systems such as rotating heat exchangers and annular cooling channels, which justify the use of this numerical approach. The applied boundary conditions in this investigation consisted of that velocity at the inlet was specified as uniform velocity inlet (with bulk velocity U_b), which was based on the studied range of Reynolds numbers. In contrast, the pressure outlet boundary condition was set to the atmospheric pressure at the exit of outlet. The inlet temperature of the working fluid (Shear-thining) was imposed at 298 K. The inner cylinder wall was heated to a constant uniform temperature of 323 K, and the outer cylinder was set adiabatic with no-slip velocity conditions. Pressure-velocity coupling was handled using the coupled algorithm, while convective terms were discretized with a second-order upwind scheme. Diffusive terms in the momentum and energy equations were approximated using a second-order central difference scheme. The default relaxation factors provided by ANSYS Fluent were 0.3 for pressure, 0.7 for momentum, and 1.0 for energy equations, as per the default settings in ANSYS Fluent 2021R1. Double-precision computations minimized numerical round-off errors and numerical convergence was ensured by terminating the iterative process once the scaled residuals of

velocity components and continuity reached (10^{-6}).

2.1 Details of the physical model

The present study aims to develop laminar flow using a three-dimensional (3D) simulation domain. As an initial step in this computational study, the flow within smooth concentric and eccentric annular cylinders is analyzed. The annular domain consists of a fixed outer cylinder with a diameter D_0 of 10 cm, while the inner cylinder diameter D_i varies in eccentricity (ε = 0.2, 0.4, 0.6), at radios ratio (r^* = 0.5). The annular gap is filled with a shear-thinning non-Newtonian fluid. This study employs a three-dimensional (3D) numerical simulation to capture the full complexity of the flow and heat transfer behavior within the annular geometry. The 3D domain is essential to resolve the axial (z-direction), radial (r-direction), and azimuthal (φ-direction) variations of velocity and temperature, especially under conditions involving inner cylinder rotation and geometric eccentricity. The temperature distribution of the working fluid was solved using the energy equation in its complete 3D form, accounting for axial conduction and convective transport. Thermal boundary conditions were applied as follows: a constant temperature (isothermal) was imposed on the inner cylinder wall, while the outer cylinder was treated as adiabatic.
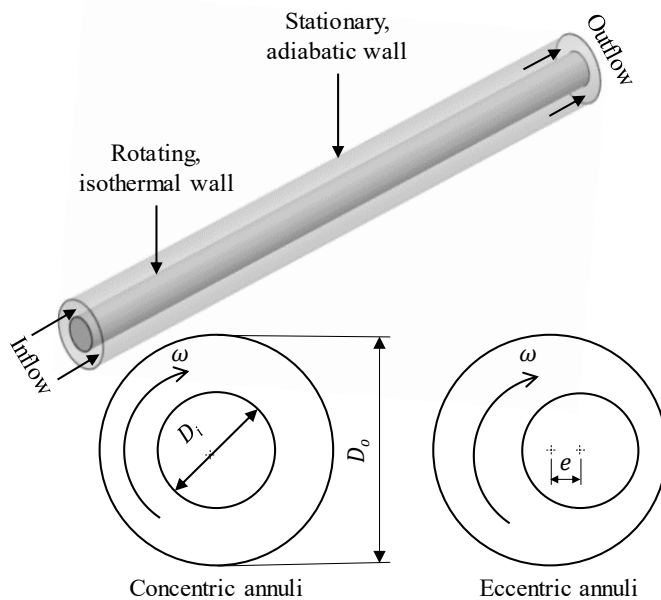

Figure 1: Schematic diagram of the concentric and eccentric annular cylinders.

This setup enables the accurate prediction of secondary flows, asymmetric velocity fields, and localized thermal gradients resulting from eccentric configurations and rotational effects.

2.2 Assumptions governing equations

In this study, the flow is assumed to be steady, laminar, and incompressible. A three-dimensional computational domain was adopted to capture the full spatial variations of velocity and temperature fields. The fluid follows a shear-thinning behavior described by the Power-law model. The inner cylinder rotates at a constant angular velocity while the outer cylinder remains stationary. Thermal boundary conditions include an isothermal inner wall (323 K) and an adiabatic outer wall (298 K). Gravitational effects are neglected, and all thermophysical properties are considered constant. The governing equations describing the three-dimensional annular flow field are formulated in cylindrical coordinates (r, φ, z), where r denotes the radial direction, φ denotes the tangential direction, and z represents the axial direction along the annular length, and comprise the conservation of mass (the continuity equation), the momentum equations (including radial, tangential, and axial components), and the energy equation. These equations are solved subject to the following constraints and assumptions: Therefore, a cylindrical coordinate system (r, φ, z) of governing equations can be summarized as[33]:

Continuity equation

$$\frac{1}{r}\frac{\partial(rv)}{\partial r} + \frac{1}{r}\frac{\partial u}{\partial \varphi} + \frac{\partial w}{\partial z} = 0 \tag{2}$$

Radial momentum equation

$$\left(v\frac{\partial v}{\partial r} + \frac{u}{r}\frac{\partial v}{\partial \varphi} + w\frac{\partial v}{\partial z} - \frac{u^2}{r}\right) = -\frac{\partial P}{\partial r}$$

$$+ \left(\frac{1}{r}\frac{\partial(r\tau_{rr})}{\partial r} + \frac{1}{r}\frac{\partial \tau_{\varphi r}}{\partial \varphi} - \frac{\tau_{\varphi\varphi}}{r} + \frac{\partial \tau_{zr}}{\partial z}\right) \tag{3}$$

Tangential momentum equation

$$\rho\left(v\frac{\partial u}{\partial r} + \frac{u}{r}\frac{\partial u}{\partial \varphi} + w\frac{\partial u}{\partial z} + \frac{uv}{r}\right) = -\frac{1}{r}\frac{\partial P}{\partial \varphi}$$

$$+ \left(\frac{1}{r^2}\frac{\partial(r^2\tau_{r\varphi})}{\partial r} + \frac{1}{r}\frac{\partial \tau_{\varphi\varphi}}{\partial \varphi} + \frac{\partial \tau_{z\varphi}}{\partial z}\right) \tag{4}$$

Axial momentum equation

$$\rho \left(v \frac{\partial w}{\partial r} + \frac{u}{r} \frac{\partial w}{\partial \varphi} + w \frac{\partial w}{\partial z} \right) = -\frac{\partial P}{\partial z}$$

$$+ \left(\frac{1}{r} \frac{\partial (r\tau_{rz})}{\partial r} + \frac{1}{r} \frac{\partial \tau_{\varphi z}}{\partial \varphi} + \frac{\partial \tau_{zz}}{\partial z} \right) \tag{5}$$

Energy equation

$$\left(v \frac{\partial T}{\partial r} + \frac{u}{r} \frac{\partial T}{\partial \varphi} + w \frac{\partial T}{\partial z} \right) =$$

$$\alpha \left(\frac{1}{r} \frac{\partial}{\partial r} \left(r \frac{\partial T}{\partial r} \right) + \frac{1}{r^2} \frac{\partial^2 T}{\partial \varphi^2} + \frac{\partial^2 T}{\partial z^2} \right) \tag{6}$$

2.3   Related non-dimensional parameters

In this study, shear-thinning non-Newtonian fluids are represented using the power-law viscosity model, where viscosity is a time-independent function of the shear rate. The governing equations for concentric and eccentric annular flow are solved computationally, providing a framework for analyzing fluid behavior. Velocity components (u_r, u_φ, u_z) correspond to radial, tangential, and axial directions, while r, φ, and z define the cylindrical coordinates.

$$\dot{\gamma}^2 = 2 \left[\left(\frac{\partial v}{\partial r} \right)^2 + \left(\frac{1}{r} \frac{\partial u}{\partial \varphi} + \frac{v}{r} \right)^2 + \left(\frac{\partial w}{\partial z} \right)^2 \right]$$

$$+ \left[r \frac{\partial}{\partial r} \left(\frac{u}{r} \right) + \frac{1}{r} \frac{\partial v}{\partial \varphi} \right]^2 + \left[\frac{1}{r} \frac{\partial w}{\partial \varphi} + \frac{\partial u}{\partial z} \right]^2 + \left[\frac{\partial v}{\partial z} + \frac{\partial w}{\partial r} \right]^2 \tag{7}$$

The Fanning friction factor (f) is derived from the balance of forces across the flow cross-section and its relation to wall shear stress (τ_w) and the hydraulic diameter (D_h). It is expressed as:

$$f = \frac{\tau_w}{\frac{1}{2} \rho U_b^2} = -\frac{\Delta P}{\rho U_b^2} \frac{D_h}{L} \tag{8}$$

Metzner and Reed [33] Introduced the concept of a generalized Reynolds (Re_g) number, which serves as a criterion for laminar flow in non-Newtonian fluids within arbitrary cross-sectional geometries. For shear-thinning fluids, its expression is given as:

$$Re_g = \frac{\rho U_b^{2-n} D_h^n}{8^{n-1} K \left(C_2 + \frac{C_1}{n} \right)^n} \tag{9}$$

where U_b is the bulk velocity, The geometric parameters C_1 and C_2, which are functions of the radius ratio $r^*(R_i/R_O)$, were determined by Kozicki et al. [34] based on the Rabinowitsch–Mooney equation, and are expressed as follows:

$$C_1 = \frac{(1-r^*)^2}{4 \left\{ 1 - \frac{1-r^{*2}}{2ln\left(\frac{1}{r^*}\right)} \left[1 - ln\left(\frac{1-r^{*2}}{2ln\left(\frac{1}{r^*}\right)} \right) \right] \right\}} \tag{10}$$

and,
$$C_1 + C_2 = \left(\frac{(1-r^*)^2}{1 + r^{*2} - \frac{1-r^{*2}}{ln\left(\frac{1}{r^*}\right)}} \right) \tag{11}$$

The axial and rotational Reynolds numbers are defined as follows:

$$Re = \frac{\rho U_b D_h}{\mu_F} \tag{12}$$

$$Re_R = \frac{\rho \omega R_i (R_o - R_i)}{\mu_F} \tag{13}$$

where μ_F is the characteristic viscosity. The Taylor number, reflecting rotational effects, is expressed as:

$$Ta = \left(\frac{\rho \omega}{\mu_F} \right)^2 R_i (R_o - R_i)^3 = \left(\frac{R_o}{R_i} - 1 \right) Re_R^2 \tag{14}$$

In the case of axial flow through an annular geometry with a rotating inner cylinder, the Reynolds and Taylor numbers are modified as:

$$Re = (1 + \xi^2)^{(1-n)/2} Re_0 \tag{15}$$

$$Ta = \left(\frac{1}{\xi^2} + 1 \right)^{1-n} Ta_0 \tag{16}$$

where ξ represents the ratio of the angular and axial velocities

$$\xi = \frac{\omega R_i}{U_b} \tag{17}$$

The average Nusselt number for the constant wall temperature at the inner wall $\overline{Nu}$ is calculated at z-direction as:

$$\overline{Nu} = \frac{hD}{k} = \frac{D_h}{(T_w - T_b)} \left(-\frac{\partial T}{\partial r} \right) \tag{18}$$

Where: The hydraulic diameter D_h is defined as $D_h = 2(R_O - R_i)$, and this definition remains valid even in the eccentric case, as the overall gap width does not change with eccentricity.

Eccentricity is defined as follow:

$$\varepsilon = e/\delta \qquad (19)$$

Where e is the displacement from inner-cylinder center to outer-cylinder center. δ is the mean annular gap width, $(R_O - R_i)$.

2.4   Mesh generation and grid sensitivity

Mesh generation is a crucial step in numerical simulations, ensuring an accurate representation of flow and heat transfer. The geometry of the annular cylinder was generated and meshed using Design Modeler within ANSYS Workbench. The Multizone meshing method was applied, generating a structured hexahedral mesh with inflation layers on the inner cylinder to improve accuracy near the boundaries while maintaining a well-organized grid. The mesh quality was evaluated based on orthogonality and skewness, with maximum and average values recorded as (0.99983, 0.90908) and (0.44554, 0.22035), respectively, ensuring numerical stability. To assess the impact of mesh refinement, a Grid Independence Test (GIT) was performed by varying the number of cells from 300,000 to 2.0 million. The results showed that beyond a certain refinement level, increasing the number of cells did not yield noticeable improvements in accuracy but led to higher computational costs. Therefore, a mesh with 1.0752 million cells was selected as the optimal choice, striking a balance between computational efficiency and numerical accuracy. The final mesh consisted of approximately 1.075 million cells, offering a balance between computational cost and numerical   accuracy. Figure 2 illustrates the generated mesh, showing the structured hexahedral elements and boundary inflation layers. A grid sensitivity analysis was conducted to assess mesh independence by varying the total number of cells from 0.3 million to 2 million. Figure 3 shows the variation of Nu and *free* concerning cell count, confirming convergence beyond the selected mesh size. The following section presents the simulation results derived using the described computational setup.
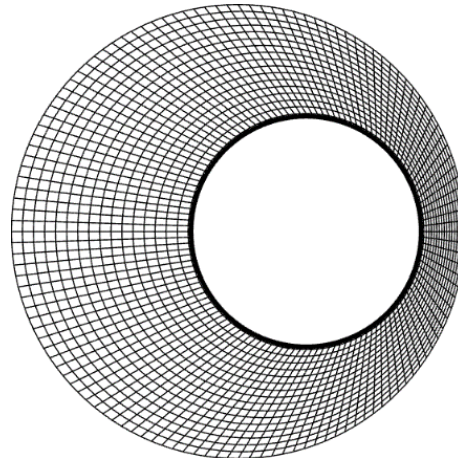

Figure 2: Nonuniform computational grid for an eccentric annular duct with a radius ratio of $r^* = 0.5$ for the chosen mesh with around one million computational cells.
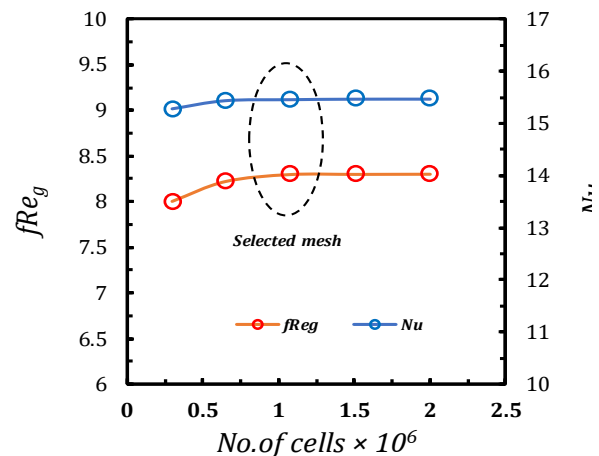

Figure 3. Mesh sensitivity test for an eccentric annular cylinder with varying numbers of cells at $r^* = 0.5$, $Re_g = 1000$, $\varepsilon = 0.6$.

3   Results and Discussion

Based on the numerical setup described above, the following section presents the computed flow and thermal characteristics.

3.1   Validation

To validate the numerical solution's accuracy that developed in this study, the obtained average Nusselt number (Nu) and Fanning friction factor-generalized Reynolds number (fRe_g) for the fully-developed power-law non-Newtonian fluid are compared with equivalent results from the prior literature. As presented in Table 1, the maximum numerical deviation from fRe_g is less than 2.2%. Additionally, the calculated Nusselt number under

boundary conditions of constant inner wall temperature and adiabatic outer wall, for various flow behavior indexes and an aspect ratio of 0.5, against the results from Refs. [22] and [27]. The agreement is reasonable, with deviations not exceeding 1.4%.

Table 1. Results of Nu and fRe_g for a fully-developed region with aspect ratio of 0.5 and different flow behavior indexes.
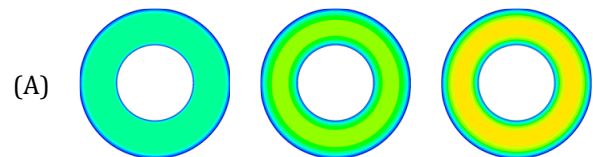
n	Source	fRe_g	Nu
	Escudier et al. [10]	3.8874	------
0.2	Manglik and Fang [22]	3.8369	5.7684
	Sefid and Izadpanah[21]	------	5.6911
	Present study	3.976	5.7678
	Escudier et al. [10]	7.9994	------
0.5	Manglik and Fang [22]	7.9395	5.7621
	Sefid and Izadpanah[21]	------	------
	Present study	8.0481	5.7598
	Escudier et al. [10]	15.438	------
0.8	Manglik and Fang [22]	15.450	5.745
	Sefid and Izadpanah[21]	------	5.6615
	Present study	15.587	5.7419
	% Max deviation	2.2	1.4

The present work investigates how the rotation of the inner cylinder and eccentricity affect both the fluid dynamics and convective heat transfer behavior of Shear-thinning non-Newtonian fluids under laminar, developing, and forced convection conditions. The analysis is conducted for generalized Reynolds numbers ($10 \leq Re_g \leq 1000$), flow behavior indexes ($0.2 \leq n \leq 0.8$), and a Taylor number ($Ta = 10^4$), considering an annular radius ratio ($r^* = 0.5$) with varying eccentricities ($0 \leq \varepsilon \leq 0.6$). For shear-thinning fluids ($n < 1$), the reduction in viscosity as the shear rate increases. Therefore, the effects of Re_g, n, ε, Ta, and thermal boundary condition on the friction factor, velocity and temperature distributions, and Nusselt number are presented here.

3.2 Power-law flow behaviour

The axial velocity contours presented in Figure 4 illustrate the influence of the flow behavior index (n), inner cylinder rotation, and eccentricity (ε) on the velocity distribution within the annular duct at $Re_g = 1000$. The results indicate that for shear-thinning fluids ($n < 1$), the velocity field exhibits significant variation due to the reduction in viscosity at high shear regions. At lower value

($n = 0.2$), the velocity distribution remains relatively uniform, whereas for higher value ($n = 0.8$), the flow becomes more localized, with high-velocity zones concentrated near the wider annular gap. The inner cylinder's rotation at $Ta = 10^4$ induces centrifugal forces, which enhance velocity gradients, particularly in the presence of eccentricity. At concentric conditions ($\varepsilon = 0$), the flow remains symmetric; however, increasing eccentricity ($\varepsilon > 0$) disrupts this symmetry, shifting the high-velocity regions toward the wider narrower section. This effect becomes more pronounced for shear-thinning fluids, where the reduced viscosity enhances velocity variations, leading to intensified shear regions and asymmetric flow structures. Figure 5 illustrates the variation of the friction factor–generalized Reynolds number product (*free) with eccentricity (ε) for various values of the generalized Reynolds number (Re_g) and flow behavior index (n) at a radius ratio ($r^* = 0.5$) and Taylor number ($Ta = 10^4$). Overall, fRe_g exhibits a decreasing trend with increasing ε, driven by changes in velocity and shear stress distributions due to the loss of geometric symmetry. As eccentricity increases, the annular gap becomes asymmetric, concentrating flow on the broader region and modifying wall shear. For shear-thinning fluids ($n = 0.2$), fRe_g remains relatively stable due to viscosity reduction in high-shear zones. In contrast, for fluids with $n = 0.8$, fRe_g decreases more noticeably with ε, especially at higher Re_g, due to their weaker shear-thinning response. Notably, at $\varepsilon = 0.6$, the redistribution of flow toward the wider region results in reduced wall shear and hydrodynamic resistance for Newtonian-like fluids. In addition, at low Reynolds numbers ($Re_g = 100$) combined with inner cylinder rotation, centrifugal forces develop that act radially outward. These forces hinder axial flow and create resistance in the narrow gap, leading to a slight increase in fRe_g. However, as eccentricity increases particularly at $\varepsilon = 0.6$, this frictional resistance decreases again due to enhanced flow redistribution and reduced confinement, especially in shear-thinning fluids.
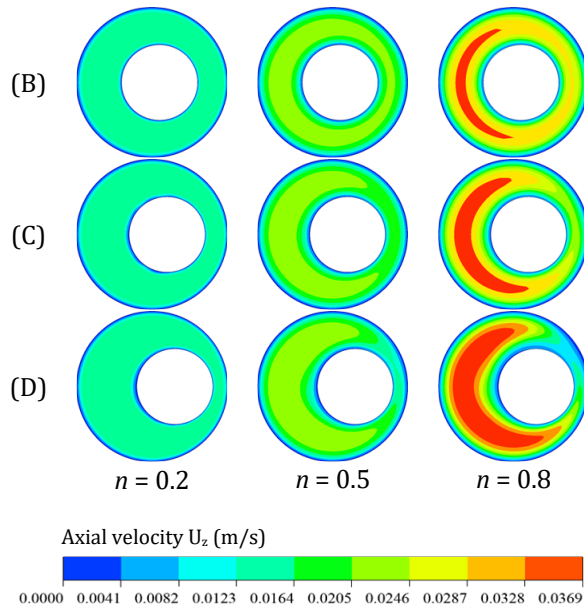
(A)

Figure 4: Cross-section contours of axial velocity fields for different flow behavior indexes (n) and eccentricities of (A) ε = 0, (B) ε = 0.2, (C) ε = 0.4, and (D) ε = 0.6, at r^*= 0.5, Re_g = 1000, and Ta = 10^4.
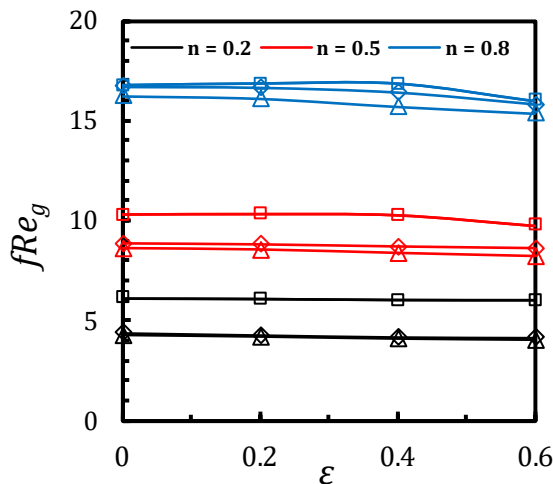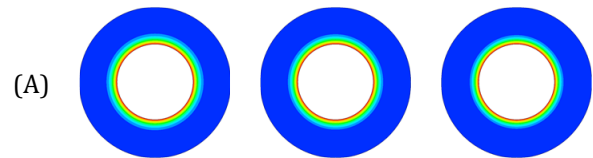

Figure 5: Influence of generalized Reynolds number and flow behavior indexes (n) on fRe_g versus ε for r^* = 0.5, Ta = 10^4, for (□) Re_g = 100, (△) Re_g = 600, (◇) Re_g = 1000.

3.3   Convective Heat Transfer Behaviour

The temperature contours in Figure 6 illustrate the influence of the flow behavior index (n) and eccentricity (ε) on heat transfer characteristics in annular geometry under inner cylinder rotation at a Taylor number of Ta = 10^4, generalized Reynolds number of Re_g = 1000, providing insights into how fluid rheology and geometric asymmetry modify the thermal field. For the concentric case

(ε = 0), the temperature distribution remains symmetric, with well-defined thermal boundary layers around the inner cylinder. The influence of flow behavior index (n) is observed. For n = 0.2, which represents a shear-thinning fluid, the viscosity decreases in high-shear regions, leading to an enhanced convective heat transfer mechanism. This effect results in a wider distribution of thermal gradients and a less localized heat transfer region, indicating improved bulk convective transport. Conversely, at n= 0.8, the viscosity remains higher, which restricts fluid motion and confines heat transfer to a thinner layer. This generates a more concentrated temperature gradient near the inner cylinder, suggesting a stronger localized heat flux. As eccentricity increases from 0.2, to 0.6, a significant asymmetry in temperature distribution emerges. At higher eccentricities, thermal gradients intensify in the narrower gap of the annular passage, where secondary flow structures promote localized heat transfer. At ε = 0.6, this effect is particularly evident, leading to stronger thermal stratification and a more pronounced contrast between high- and low-temperature regions. This localized increase in temperature gradient indicates an enhancement in heat transfer efficiency near the inner wall, despite the outer regions experiencing reduced convective transport. Additionally, the inner cylinder rotation at Ta = 10^4 plays a crucial role in modifying the thermal distribution. The rotational motion induces secondary flow patterns that interact with the effects of shear-thinning, redistributing the temperature field and enhancing heat transfer in regions of high shear. The combination of rotation and eccentricity further amplifies this effect, demonstrating that geometric asymmetry combined with rotational influence can significantly impact heat transfer efficiency. These findings suggest that while shear-thinning fluids (n = 0.2) exhibit enhanced convective transport over a broader region, fluids with higher power-law indices (n = 0.8) show intensified localized heat flux, particularly in eccentric configurations.
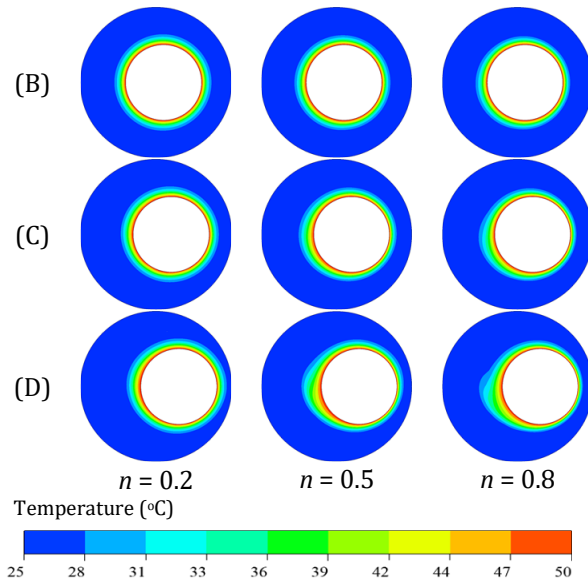
Figure 6: Cross-section contours of temperature distribution fields for different flow behavior indexes (*n*) and eccentricities (*ε*), For (A) *ε* = 0, (B) *ε* = 0.2, (C) *ε* = 0.4, (D) *ε* = 0.6, at *r** = 0.5, Re_g = 1000, *Ta* = 10^4.
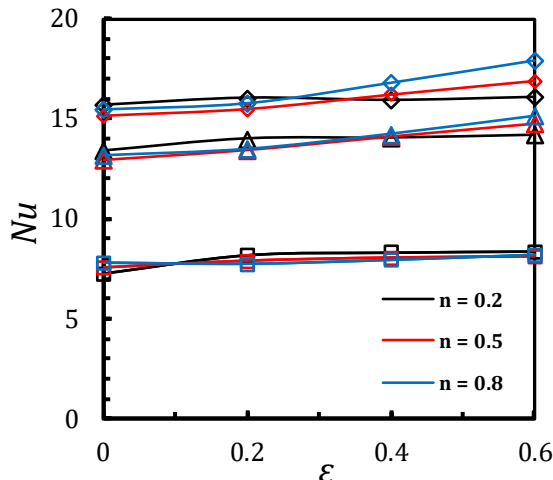

Figure 7: Effect of generalized Reynolds number and shear-thinning rheology (*n*) on *Nu* versus *ε* for *r** = 0.5, *Ta* = 10^4, (□) Re_g = 100, (△) Re_g = 600, (◇) Re_g = 1000.

Figure 7 illustrates the effect of geometric eccentricity (*ε*) on the average Nusselt number (*Nu*) at different flow behavior indices (*n*) and generalized Reynolds numbers (Re_g) under fixed inner cylinder rotation (*Ta* = 10^4) and radius ratio (*r** = 0.5). The results reveal a clear trend of increasing *Nu* with eccentricity, particularly at higher Re_g. At Re_g = 100, the enhancement in *Nu* is minimal for all *n*, indicating that conductive mechanisms dominate at low flow intensities and the influence of geometric asymmetry is limited.

However, as Re_g increases to 600 and 1000, a stronger dependence of *Nu* on *ε* is observed, especially for fluids with higher n (weaker shear-thinning behavior). In these cases, eccentricity promotes the formation of localized vortices and secondary flows near the narrow gap region, enhancing convective mixing and thinning the thermal boundary layer thereby improving heat transfer Interestingly, while shear-thinning fluids (*n* = 0.2) show higher *Nu* in concentric conditions due to their lower viscosity in high-shear zones, increasing eccentricity gradually reduces this advantage. At *ε* = 0.6, the heat transfer performance becomes more uniform across all *n*. As shown in Figure 7, the highest Nu is recorded for *n* = 0.8, Re_g = 1000. This inversion highlights the crucial role of geometric asymmetry in regulating convective transport when combined with strong rotational and inertial effects. The combined impact of eccentricity and inner cylinder rotation can overcome rheological limitations and significantly enhance thermal performance in annular configurations.

4   Conclusion

This study presented a three-dimensional numerical investigation of developing laminar flow and heat transfer of shear-thinning non-Newtonian fluids in annular geometries, considering both inner cylinder rotation and geometric eccentricity.
1. In concentric configurations, fluids with lower power-law index (*n* = 0.2) exhibited reduced viscosity, leading to lower flow resistance and enhanced convective heat transfer.
2. Increasing eccentricity (*ε* = 0.2 – 0.6) introduced significant flow asymmetry, with peak velocity shifting toward the wider gap. At the same time, heat transfer intensified in the narrow region due to elevated shear rates and thermal gradients.
3. Interestingly, at high eccentricity (*ε* = 0.6), fluids with a higher power-law index (n = 0.8) achieved the highest average Nusselt number contrary to typical shear-thinning behavior due to the emergence of strong secondary flows that enhanced thermal mixing.
4. The (*fRe_g*) did not consistently decrease with increasing Reynolds number. In some cases, particularly at high eccentricity and *Ta* = 10^4, vortex-induced circulations contributed to a local increase in hydrodynamic resistance.
5. Among all examined cases, the configuration with *ε* = 0.6, *n* = 0.8, and Re_g = 1000 demonstrated the best thermal performance due to intensified

secondary flow structures; the lowest (fRe_g) was observed at $n = 0.2$ for high Reynolds numbers, with only a slight decrease in fRe_g as eccentricity increased.

Finally, while the present study provides valuable insights into the hydrothermal behavior of shear-thinning fluids in annular configurations, future research may expand the scope by exploring alternative rheological models, varying thermal boundary conditions, and a broader range of geometric parameters. These efforts would further align the study with diverse engineering applications mentioned in the introduction.

References

[1] F. A. Morrison, *Understanding Rheology*. 2001.

[2] J. F. R. R. P. Chhabra, *Non-Newtonian Flow and Applied Rheology: Engineering Applications*. 2011.

[3] H. A. Barnes, J. F. Hutton, and K. Walters, *An Introduction to Rheology*, no. vol. 3. in An Introduction to Rheology. Elsevier Science, 1989.

[4] O. H. R. Byron Bird, Robert C. Armstrong, *Dynamics of polymeric liquids*, 2nd ed. New York: Wiley, 1987.

[5] R. J. Poole, "Inelastic and flow-type parameter models for non-Newtonian fluids," *J. Nonnewton. Fluid Mech.*, vol. 320, p. 105106, Oct. 2023, doi: 10.1016/j.jnnfm.2023.105106.

[6] P. J. Carreau, "Rheological Equations from Molecular Network Theories," *Trans. Soc. Rheol.*, vol. 16, no. 1, pp. 99–127, Mar. 1972, doi: 10.1122/1.549276.

[7] M. M. Cross, "Rheology of non-Newtonian fluids: A new flow equation for pseudoplastic systems," *J. Colloid Sci.*, vol. 20, no. 5, pp. 417–437, Jun. 1965, doi: 10.1016/0095-8522(65)90022-X.

[8] K. Yasuda, R. C. Armstrong, and R. E. Cohen, "Shear flow properties of concentrated solutions of linear and star branched polystyrenes," *Rheol. Acta*, vol. 20, no. 2, pp. 163–178, Mar. 1981, doi: 10.1007/BF01513059.

[9] M. P. Escudier, I. W. Gouldson, A. S. Pereira, F. T. Pinho, and R. J. Poole, "On the reproducibility of the rheology of shear-thinning liquids," *J. Nonnewton. Fluid Mech.*, vol. 97, no. 2–3, pp. 99–124, Feb. 2001, doi: 10.1016/S0377-0257(00)00178-6.

[10] M. P. Escudier, P. J. Oliveira, and F. T. Pinho, "Fully developed laminar flow of purely viscous non-Newtonian liquids through annuli, including the effects of eccentricity and inner-cylinder rotation," *Int. J. Heat Fluid Flow*, vol. 23, no. 1, pp. 52–73, Feb. 2002, doi: 10.1016/S0142-727X(01)00135-7.

[11] S. H. Lin, "Heat transfer to generalized non-Newtonian Couette flow in annuli with moving outer cylinder," *Int. J. Heat Mass Transf.*, vol. 35, no. 11, pp. 3069–3075, Nov. 1992, doi: 10.1016/0017-9310(92)90326-N.

[12] H. E. Ahmed and M. I. Ahmed, "Thermal performance of annulus with its applications; A review," *Renew. Sustain. Energy Rev.*, vol. 71, no. December, pp. 170–190, 2017, doi: 10.1016/j.rser.2016.12.050.

[13] A. Davey, R. C. Di Prima, and J. T. Stuart, "On the instability of Taylor vortices," *J. Fluid Mech.*, vol. 31, no. 01, p. 17, Jan. 1968, doi: 10.1017/S0022112068000029.

[14] K. S. Ball, B. Farouk, and V. C. Dixit, "An experimental study of heat transfer in a vertical annulus with a rotating inner cylinder," *Int. J. Heat Mass Transf.*, vol. 32, no. 8, pp. 1517–1527, Aug. 1989, doi: 10.1016/0017-9310(89)90073-2.

[15] G. Zeng-Yuan and Z. Chao-Min, "Thermal drive in centrifugal fields—mixed convection in a vertical rotating cylinder," *Int. J. Heat Mass Transf.*, vol. 35, no. 7, pp. 1635–1644, Jul. 1992, doi: 10.1016/0017-9310(92)90134-E.

[16] M. P. Escudier, I. W. Gouldson, P. J. Oliveira, and F. T. Pinho, "Effects of inner cylinder rotation on laminar flow of a Newtonian fluid through an eccentric annulus," *Int. J. Heat Fluid Flow*, vol. 21, no. 1, pp. 92–103, Feb. 2000, doi: 10.1016/S0142-727X(99)00059-4.

[17] W. M. Abed, A. Al-Damook, and W. H. Khalil, "Convective heat transfer in an annulus of concentric and eccentric cylinders with an inner rotating cylinder," *Int. J. Heat Technol.*, vol. 39, no. 1, pp. 61–72, 2021, doi: 10.18280/ijht.390107.

[18] M. P. Escudier, I. W. Gouldson, and D. M. Jones, "Flow of shear-thinning fluids in a concentric annulus," *Exp. Fluids*, vol. 18, no. 4, pp. 225–238, Feb. 1995, doi: 10.1007/BF00195092.

[19] P. Escudier and I. W. Gouldson, "Configuration1 of Technical Report," no. 95, pp. 156–162, 1995.

[20] M. Escudier, P. Oliveira, F. Pinho, and S. Smith, "Fully developed laminar flow of non-Newtonian liquids through annuli: Comparison of numerical calculations with

experiments," *Exp. Fluids*, vol. 33, no. 1, pp. 101–111, 2002, doi: 10.1007/s00348-002-0429-4.

[21] M. Sefid and E. Izadpanah, "Developing and fully developed non-newtonian fluid flow and heat transfer through concentric annuli," *J. Heat Transfer*, vol. 135, no. 7, pp. 1–8, 2013, doi: 10.1115/1.4023882.

[22] R. M. Manglik and P. Fang, "Thermal processing of viscous non-Newtonian fluids in annular ducts: effects of power-law rheology, duct eccentricity, and thermal boundary conditions," *Int. J. Heat Mass Transf.*, vol. 45, no. 4, pp. 803–814, Feb. 2002, doi: 10.1016/S0017-9310(01)00186-7.

[23] R. M. Manglik and J. Prusa, "Viscous dissipation in non-Newtonian flows: Implications for the nusselt number," *J. Thermophys. Heat Transf.*, vol. 9, no. 4, pp. 733–742, 1995, doi: 10.2514/3.732.

[24] V. Salubi, R. Mahon, and G. Oluyemi, "The combined effect of fluid rheology, inner pipe rotation and eccentricity on the flow of Newtonian and non-Newtonian fluid through the annuli," *J. Pet. Sci. Eng.*, vol. 211, no. June 2021, p. 110018, 2022, doi: 10.1016/j.petrol.2021.110018.

[25] R. Ershadnia *et al.*, "Non-Newtonian fluid flow dynamics in rotating annular media: Physics-based and data-driven modeling," *J. Pet. Sci. Eng.*, vol. 185, no. November 2019, p. 106641, 2020, doi: 10.1016/j.petrol.2019.106641.

[26] [26] L. Fusi, A. Farina, and K. R. Rajagopal, "Secondary flow of an elastic-viscoplastic fluid in an eccentric annulus," *Int. J. Non. Linear. Mech.*, vol. 158, no. September 2023, p. 104564, 2024, doi: 10.1016/j.ijnonlinmec.2023.104564.

[27] B. Traore, C. Castelain, and T. Burghelea, "Efficient heat transfer in a regime of elastic turbulence," *J. Nonnewton. Fluid Mech.*, vol. 223, pp. 62–76, 2015, doi:

10.1016/j.jnnfm.2015.05.005.

[28] G. Yao, J. Zhao, X. Shen, H. Yang, and D. Wen, "Effects of rheological properties on heat transfer enhancements by elastic instability in von-Karman swirling flow," *Int. J. Heat Mass Transf.*, vol. 152, p. 119535, 2020, doi: 10.1016/j.ijheatmasstransfer.2020.119535.

[29] [29] G. Yao, H. Yang, J. Zhao, and D. Wen, "Experimental study on flow and heat transfer enhancement by elastic instability in swirling flow," *Int. J. Therm. Sci.*, vol. 157, no. May, p. 106504, 2020, doi: 10.1016/j.ijthermalsci.2020.106504.

[30] R. D. Whalley, W. M. Abed, D. J. C. Dennis, and R. J. Poole, "Enhancing heat transfer at the micro-scale using elastic turbulence," *Theor. Appl. Mech. Lett.*, vol. 5, no. 3, pp. 103–106, 2015, doi: 10.1016/j.taml.2015.03.006.

[31] D. Y. Li, X. Bin Li, H. N. Zhang, F. C. Li, S. Z. Qian, and S. W. Joo, "Measuring heat transfer performance of viscoelastic fluid flow in curved microchannel using Ti-Pt film temperature sensor," *Exp. Therm. Fluid Sci.*, vol. 77, pp. 226–233, 2016, doi: 10.1016/j.expthermflusci.2016.05.001.

[32] W. M. Abed, R. D. Whalley, D. J. C. Dennis, and R. J. Poole, "Experimental investigation of the impact of elastic turbulence on heat transfer in a serpentine channel," *J. Nonnewton. Fluid Mech.*, vol. 231, pp. 68–78, 2016, doi: 10.1016/j.jnnfm.2016.03.003.

[33] [A. B. Metzner and J. C. Reed, "Flow of Non-Newtonian Fluids-Correlation of the Laminar , Transition , and Turbulent-flow Regions," no. 4, 1955.

[34] W. Kozicki, C. H. Chou, and C. Tiu, "Non-Newtonian flow in ducts of arbitrary cross-sectional shape," *Chem. Eng. Sci.*, vol. 21, no. 8, pp. 665–679, Aug. 1966, doi: 10.1016/0009-2509(66)80016-7.

Nomenclature

D_h	hydraulic diameter, 2δ (m)	u_z	axial component of velocity (m/s)
e	displacement of inner-cylinder axis from outer-cylinder axis (m)	u_φ	tangential component of velocity (m/s)
f	Fanning friction factor	u_r	radial component of velocity (m/s)
h	heat transfer coefficient, W/m m^2 K	δ	Mean annular gap width, $R_O - R_i$(m)
k	thermal conductivity, W/m K	ε	eccentricity, e/δ
K	fluid consistency (Pa s^n)	r^*	radius ratio, R_i/R_O
n	flow behavior index	μ	dynamic viscosity (Pa s)
Nu	Nusselt number based on hydraulic diameter and heat transfer coefficient	μ_F	characteristic viscosity for flow (Pa s)
R_i	outer radius of inner cylinder (m)	ξ	velocity ratio, $\omega R_i/U_b$
R_o	inner radius of outer cylinder (m)	ω	angular velocity of inner cylinder (rad/s)
fRe_g	friction factor–generalized Reynolds number product	ρ	fluid density (kg/m^3)
r^*	radius ratio of annulus cross-section, (r_i/r_o)	$\dot{\gamma}$	shear rate (s^{-1})
Re_g	Reynolds number based on hydraulic	τ_w	wall shear stress (N/m^2)
Re	axial Reynolds number	τ_w	wall shear stress (N/m^2)
Re_R	rotational Reynolds number	$\dot{\gamma}_F$	characteristic shear rate for flow (s^{-1})
Re_0	correspond with generalised Reynolds number when $\omega = 0$, $Re_0 = \dfrac{\rho U_b^{2-n} D_h^n}{8^{n-1}K\left(C_2+\frac{C_1}{n}\right)^n}$		
Ta	Taylor number		
Ta_0	correspond with generalised Taylor number when U$_z$ = 0, $Ta_0 = \dfrac{1}{8}\left(\rho\dfrac{\omega^{2-n}}{K}\right)^2 D_h^{2n+1} R_1^{3-2n}$		
U_b	Bulk axial velocity (m/s)		